Optical Engineering

OpticalEngineering.SPIEDigitalLibrary.org

Vane structure optimization method for stray light suppression in a space-based optical system with wide field of view

Zeming Xu
Chunhui Hu
Changxiang Yan
Cang Gu

SPIE.

Zeming Xu, Chunhui Hu, Changxiang Yan, Cang Gu, "Vane structure optimization method for stray light suppression in a space-based optical system with wide field of view," *Opt. Eng.* **58**(10), 105103 (2019), doi: 10.1117/1.OE.58.10.105103.

Vane structure optimization method for stray light suppression in a space-based optical system with wide field of view

Zeming Xu,[a,b] Chunhui Hu,[a,*] Changxiang Yan,[a,c] and Cang Gu[d]
[a]Chinese Academy of Sciences, Changchun Institute of Optics, Fine Mechanics and Physics, Changchun, China
[b]University of Chinese Academy of Sciences, Beijing, China
[c]University of Chinese Academy of Sciences, Center of Materials Science and Optoelectrics Engineering, Beijing, China
[d]Changchun AoPu Photoelectric Technology Co., Ltd., Changchun, China

Abstract. To meet the requirements for the safety of the space environment and the increasing demand for the detection of faint targets in deep space, using a space-based detection optical system with a wide field of view (FOV) has become a major trend. However, such systems are very susceptible to stray light. Based on the above background, we design a baffle with angled and parallel vanes under the limitation of a miniaturized baffle, and we propose a vane angle optimization method. The method is proposed by establishing an irradiance transfer model based on the bidirectional scattering distribution function with Gaussian statistics on the surface of baffle and vane. In addition, the result of the point source transmittance (PST) obtained by Monte Carlo simulation in LightTools indicated that the PST is improved by 2 to 5 times in the FOV of 30 deg and 70 deg when the angle of incidence is at the stray light exclusive angle compared to the traditional method. Meanwhile, the method establishes an analytical expression; therefore, the optimization process is more efficient, and the time required for simulation can be significantly reduced. [DOI: 10.1117/1.OE.58.10.105103]

Keywords: stray light suppression; space-based optical system; wide of field; bidirectional scattering distribution function; baffle and vane.

Paper 191029 received Jul. 25, 2019; accepted for publication Sep. 26, 2019; published online Oct. 18, 2019.

1 Introduction

Having a wide field can effectively improve the ability of a space surveillance telescope to detect faint space targets. To meet the requirements for the safety of the space environment and the increasing demand for the detection of faint targets in deep space, using a space-based detection optical system with a wide field of view (FOV) has become a major trend, given the Fengyun Satellite,[1] the Midcourse Space Experiment Spacecraft,[2,3] and the Space-Based Space Surveillance Project.[4,5] Because such space optical systems are used to detect faint targets, they are susceptible to the effects of the Sun, Moon, and Earth, and the radiance of these stray light sources is always higher than targets by several orders of magnitude. If stray light cannot be effectively suppressed, the image quality and target resolution degrades dramatically or even leads to the direct failure of the space optical system.[6–8]

To reduce the interference of stray light sources outside the FOV, the common method is to design a baffle with vanes to suppress stray light. Before entering the lens, the stray light should be scattered at least two times in the baffle structure. In terms of baffle design, there have been many methods proposed and applied in past decades, such as designing a multistage baffle,[9] designing the chamfering and inclination of vanes,[10,11] using reflective vanes with a symmetric curve,[12] using an asymmetric baffle structure in special orbits,[13,14] and programing the baffle and vanes design.[15,16] Although these methods have achieved considerable success, they are only for stray light with scattering once and based on the geometry principle.[17] Generally, we do not worry about the vane angle optimization because we focus on other aspects of the vane structure (thickness, shape, edge geometry, and orientation). However, vane angle optimization is very important for improving the performance of stray light suppression in the space-based system of this paper. On the one hand, the optical specifications necessary for the space-based system are a wide FOV of 30 deg × 70 deg, a focusing length of 185 mm, and an entrance pupil diameter of 55 mm. It is generally not possible to implement a multistage baffle on the space-based system with a wide FOV because that would make the baffle occupy a very large volume.[17] On the other hand, because the edge of the vane is sharp[18] and the absorptivity of the baffle and vane is always between 95% and 97%,[19,20] the second-level scatter light has huge interference on the limitation of a miniaturized baffle and the detection of faint targets. Specifically, about 93% of the energy entering into the lens comes from the second-level scatter light in the preliminary analysis. We can reduce the interference of the second-level scatter light by optimizing the vane angle instead of increasing the length of the baffle. Therefore, vane angle optimization is very important for shrinking the volume of the baffle and improving the stray light suppression performance in this system.

In this paper, we designed a baffle with angled and parallel vanes under the limitation of a miniaturized baffle, and we proposed a novel vane structure optimization method to shrink the volume of the baffle and improve the performance of stray light suppression. The method was proposed by

*Address all correspondence to Chunhui Hu, E-mail: hchciomp@163.com

0091-3286/2019/$28.00 © 2019 SPIE

establishing an irradiance transfer model based on the bidirectional scattering distribution function (BSDF) with Gaussian statistics on the surface of baffle and vane. Furthermore, this method can greatly reduce the time required for the optimization process, and the result of the point source transmittance (PST) obtained by Monte Carlo ray-tracing simulation in LightTools indicated that it was consistent with the calculation result based on the method, and the PST was improved by 2 to 5 times in the x direction FOV and y direction FOV when the angle of incidence was at the stray light exclusive angle compared with the traditional method. In addition, the baffle had a small length of 80 mm instead of 98 mm by this optimization method.

2 Stray Light Suppression Method

2.1 *Theory of Stray Light Suppression*

Generally, vanes are used in the baffle to increase the scatter times before the stray light enters the lens to improve the performance of stray light suppression. There are two kinds of vanes structures for the baffle (angled vanes and vertical vanes), and the angled vanes can shrink the baffle size and have better performance on stray light elimination than the vertical vanes.[18] The number of vanes is related to the length and width of the baffle, and the principle of the minimum vanes is that the sidewall cannot be directly viewed from the lens.[17,18] In this paper, to facilitate the processing, we still use parallel vane structures, and five angled vanes are employed in the FOV of 30 deg and thirteen angled vanes are employed in the FOV of 70 deg. The lengths of vanes and the distance between vanes are determined by the traditional geometrograph method.[17] However, different from the geometrograph method, the angle range between the vane and baffle is determined by the boundary incident light line at the first and last vanes, FOV line, and sidewall of the baffle; and the baffle design of 30-deg FOV is shown in Fig. 1. AA′ and BB′ denote the exit and the entrance of the baffle separately, and CC′ denotes the angle variation range of the vanes (when the vane angle is not in this angle variation range, the first-level scatter light will enter the lens directly), red part of the vanes and the baffle denote the visible areas of the lens when the incident angle of the light is greater than the stray exclusive angle, and κ_1–κ_5 denote the angle between the visible areas and the system optical axis. Similarly, the baffle design of the 70-deg FOV can also be achieved in the same way.

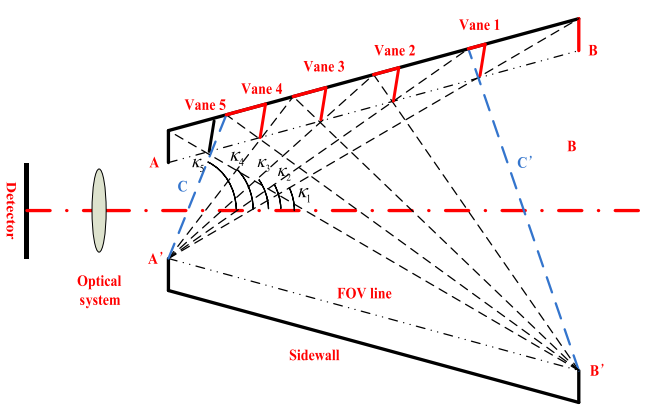

Fig. 1 Cutaway view of the space-based optical system and the baffle with angled vanes in a 30-deg FOV.

In order to improve the performance of stray light suppression and shrink the length of the baffle, we should design a suitable vane angle within the angle range. Because when the angle is greater than the angle range, plenty of first-level scatter light will access into the lens. A suitable vane angle can block a lot of second-level scatter light. Meanwhile, the edge of the vane should be sharp.[18,19] Before optimizing the vane angle, we should establish the scattering model of the baffle and vane. Because the scattering characteristic of the surface determines the propagation characteristics of light, it is the basis for optimizing the vane angle.

2.2 *BSDF Model of the Baffle and Vane*

We usually use the BSDF to represent the scattering characteristics, as shown in Fig. 2. The BSDF defines the ratio of the scattering radiance to the incident irradiance for rough surface, as shown in

$$\mathrm{BSDF}(\theta_i,\theta_s,\varphi_i,\varphi_s)=\frac{L_s(\theta_s,\varphi_s)}{E_i(\theta_i,\varphi_i)}. \tag{1}$$

Here θ_i and φ_i are the polar and azimuthal angles of the incident light direction, and θ_s and φ_s are the polar and azimuthal angles of the scattering (outgoing) light direction.

Therefore, establishing an accurate and suitable BSDF model is the primary condition for quantitative analysis of stray light. However, analytically deriving a BSDF model is very difficult. There are multiple factors involved, including the incident and outgoing directions, material roughness, material composition, wavelength, and polarization.[21] Because this is not the main content of this paper, we use the scattering model established in the literature and select the appropriate parameters based on the situation in this paper.[21–25] The BSDF model established in the literatures is based on Gaussian statistics of the surface, and the BSDF model is shown in the following equation:[21–25]

$$\mathrm{BSDF}(\theta_i,\theta_s,\varphi_i,\varphi_s)=\frac{M^2F\exp(-S^2\tan^2\theta_h/4)}{16\pi\cos\theta_i\cos\theta_s\cos^4\theta_h}V(\theta_i)V(\theta_s),$$
$$M=\frac{\tau}{\sigma}, \tag{2}$$

where θ_i and φ_i are the polar and azimuthal angles of the incident light direction, respectively; θ_s and φ_s are the polar and azimuthal angles of the scattering (outgoing) light direction; F is the absorptivity of the baffle and vane; σ and τ represent the root-mean-square roughness and coherence

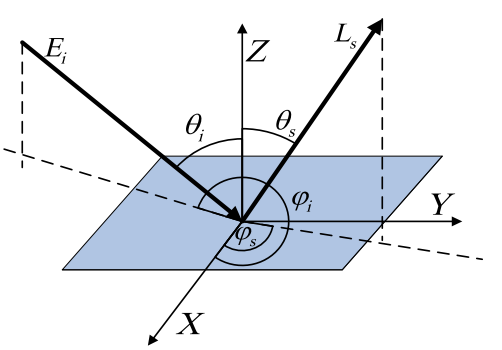

Fig. 2 Geometry and notations for defining the BSDF.

length of surface, respectively; and θ_h is the angle between the microfacet normal and the macrosurface normal. θ_h can be obtained by the following equation:

$$\cos\theta_h = \frac{\cos\theta_i + \cos\theta_s}{\sqrt{2+2\cos 2\varepsilon}}$$
$$\cos 2\varepsilon = \sin\theta_i \sin\theta_s \cos(\varphi_i - \varphi_s) + \cos\theta_i \cos\theta_s. \quad (3)$$

$V(\theta_i)$ and $V(\theta_s)$ are the visibility functions of the incident and scattering light, respectively. They indicate the blocking effect for incident light and scattering (outgoing) light, and they can be obtained by the following equation:

$$V(\theta_i) = \exp\left[-\frac{7\tan\theta_i}{10M}\exp\left(-\frac{M^2}{\tan^2\theta_i}\right)\right]$$
$$V(\theta_s) = \exp\left[-\frac{7\tan\theta_s}{10M}\exp\left(-\frac{M^2}{\tan^2\theta_s}\right)\right]. \quad (4)$$

Through analysis, we will select the appropriate parameters (F and M) to match the actual scattering characteristics of the baffle and vane in this space-based optical system. Figure 3 shows the BSDF distribution at different incident angles.

After establishing the BSDF model, the angle of the vane structure can be designed by the following optimization method as follows.

3 Vane Angle Optimization Method for Stray Light Suppression

The traditional vane structure is a vertical structure, i.e., perpendicular to the optical axis of the system. Generally, we do not think about the problem of vane angle. However, the space-based system has a wide FOV of 30 deg × 70 deg in the x direction FOV and y direction FOV, and we can only design a miniaturized baffle with one stage (as shown in Fig. 1) to meet the requirement of the size indicator in this system. In addition, our space-based optical system is a monocentric lens imaging system using fiber-coupled focal planes, through a "virtual stop" formed by fiber-coupled focal planes limits almost all margin scattering.[26–28] Compared to the second-level scatter light, the intensity of margin scattering is two orders of magnitude lower. The second-level scatter light is the main source of stray light in this one stage baffle.[29] The proportion of the second-level scatter light accounts for more than 93%, its intensity is more than two orders of magnitude higher than other scattering components. Therefore, the optimization of the vane angle is the only way to reduce the size of the baffle without decreasing stray light suppression performance, which the parameters of the miniaturized baffle in the space-based system are shown in Table 1.

Table 1 The parameters of a miniaturized baffle.

Direction	Exit aperture (mm)	FOV (deg)	Stray light exclusive angle (deg)
X	70	30	50
Y	90	70	70

To determine the efficiency of stray light suppression, we usually define the parameter PST function:

$$\mathrm{PST}(\omega) = \frac{E_{\mathrm{detector}}}{E_{\mathrm{baffle}}}, \quad (5)$$

where E_{baffle} is the irradiance of light entering the baffle at angle ω, and E_{detector} is the maximized irradiance on the detector. We can reduce the PST by optimizing the angle of the angled vane structure. The traditional Monte Carlo ray-tracing simulation is always used for optimizing the angle. However, this method is very inefficient and time-consuming because we need a new simulation circumstance and mechanical

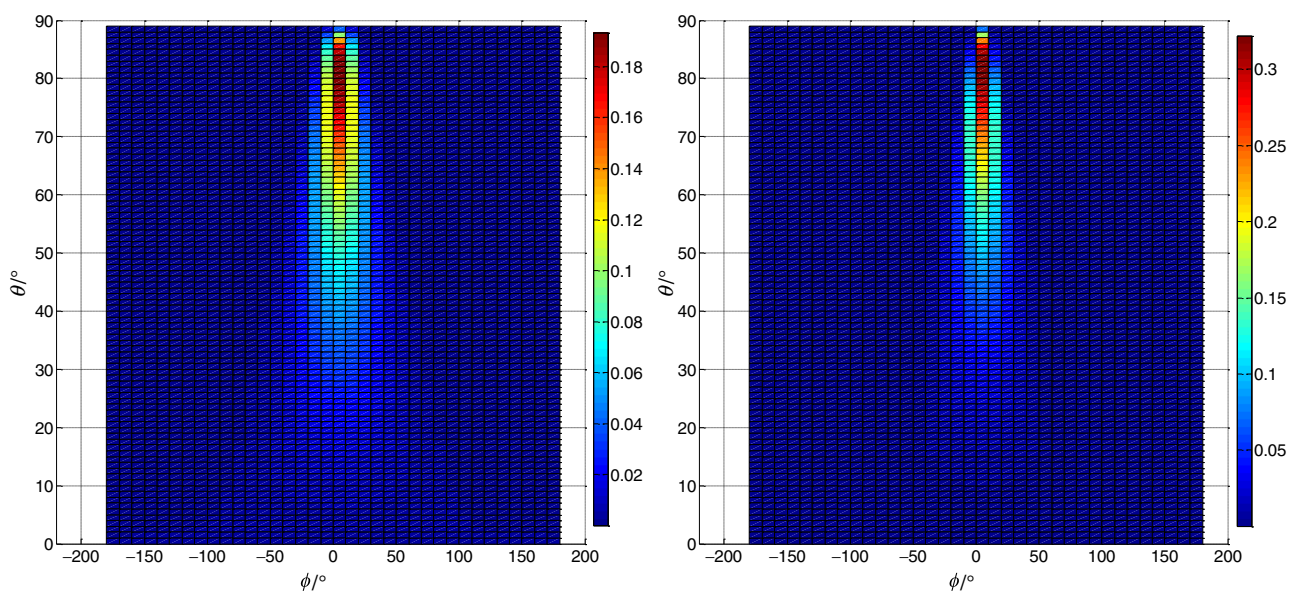

Fig. 3 The BSDF distribution with the polar (θ) and azimuthal (φ) angles of the scattering (outgoing) light direction at different angles: (a) the polar (50 deg) and azimuthal (180 deg) angles of the incident light direction and (b) the polar (70 deg) and azimuthal (180 deg) angles of the incident light direction.

structure for each simulation and the tracing result requires many light rays. Therefore, we established an irradiance transfer model with analytical expressions to effectively and rapidly optimize the vane angle and reduce the PST. In addition, as mentioned above, the proportion of the second-level scatter light accounts for more than 93%, so we only considered the second-level scatter light in this model. According to the practical propagation process of light ray and the scattering characteristic on the surface of the vane and baffle, the maximized irradiance on the detector can be calculated with the following equation:

$$E_d = \sum_{1}^{n} E_i, \tag{6}$$

where E_d denotes the total irradiance on the detector with scattering twice, and E_i denotes the maximized irradiance on the detector that comes from the visible areas (the red part of Fig. 1). In addition, while this system has a larger FOV, the intensity of light scattered into the opposite visible areas is reduced by more than an order of magnitude in the preliminary analysis. Thus the irradiance from the opposite visible areas is so small that we do not need to consider it. Therefore, the PST can be calculated with the following equation:

$$\mathrm{PST}(\omega) = \frac{E_d}{E_b} = \sum_{1}^{n} \mathrm{PST}_i(\omega), \tag{7}$$

where E_b denotes the irradiance of entering the baffle at a stray light exclusive angle, PST_i denotes the PST of each visible area (the red part of Fig. 1). This process is analyzed in Secs. 3.1 and 3.2.

3.1 *BSDF Model of Second-Level Scatter Light*

The practical propagation path of the light ray is scattered to the stereoscopic space after being absorbed by the surface material, and the scattering characteristic is described by the BSDF model in Sec. 2.2. There are four parameters $(\theta_i, \theta_s, \varphi_i, \varphi_s)$ that affect the distribution of scattered light, and there are more parameters when considering second-level scatter light, and we need to integrate for each scattering, causing this process to be very complicated. Therefore, the BSDF model needs to be simplified appropriately. On the one hand, the process is very difficult when it is necessary to quantify the scattering light in the stereoscopic space. However, we found that most of the scattering light is concentrated in the incident plane, and when it is more than 5 deg from the incident plane, its BSDF value is reduced by more than one order, and the proportion increases with the increased degree of deviation and the increased incident angle, as shown in Fig. 4. Therefore, the stereoscopic quantization process can be simplified to the plane quantization process.

On the other hand, for the second-level scatter light incident on the detector that comes from the visible areas (the red part of Fig. 1), there are only two kinds of propagation paths: one propagation path is when stray light scattered to the detector after passing through vane and baffle. In this condition, the first-level scatter light of vane is forward-scatter (the scattering light and incident light are on both sides of the normal) light, and the second-level scatter light of baffle is back-scatter (the scattering light and incident light are on the same side of the normal) light. Another propagation path is when stray light is scattered to the detector after passing through the vane and opposite the vane. In this condition, there are also two kinds of propagation paths: path 1 is when the first-level scatter light of vane is back-scatter (the scattering light and incident light are on the same side of the normal) light and the second-level scatter light of the opposite vane is forward-scatter (the scattering light and incident light are on both sides of the normal) light. Path 2 is when the first-level scatter light of vane is forward-scatter (the scattering light and incident light are on both sides of the normal) light, and the second-level scatter light

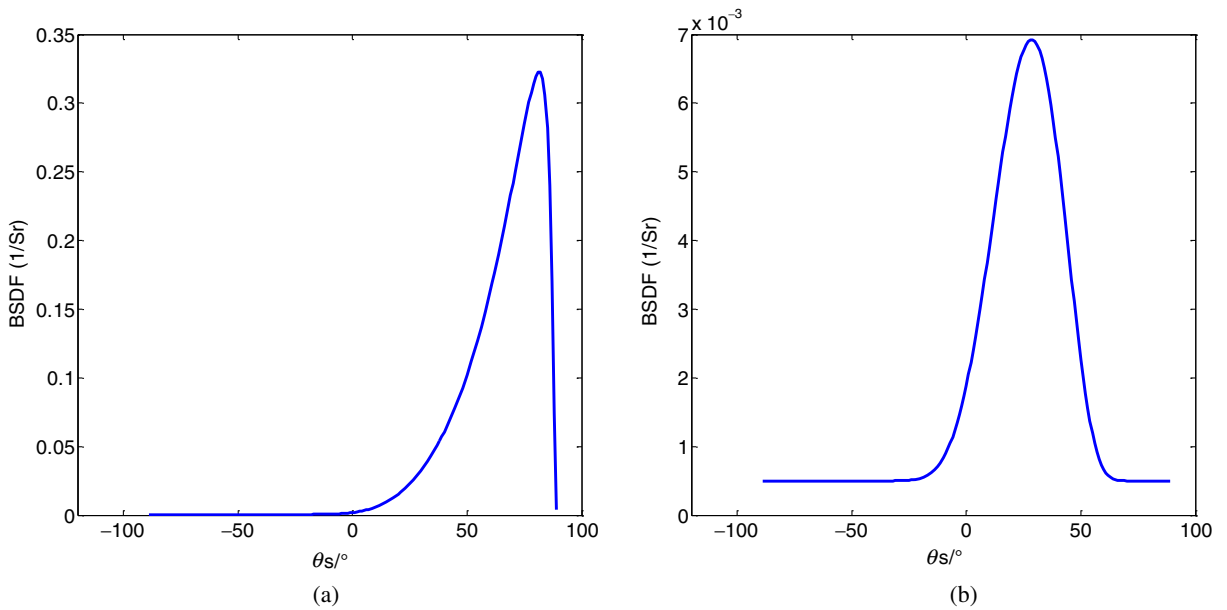

Fig. 4 BSDF distribution in different scattering planes at a 70-deg incident angle: (a) BSDF distribution in the plane of incidence and (b) BSDF distribution at an angle of 3 deg to the incident plane, where $\theta < 0$ deg denotes $\varphi_s = 180$ deg.

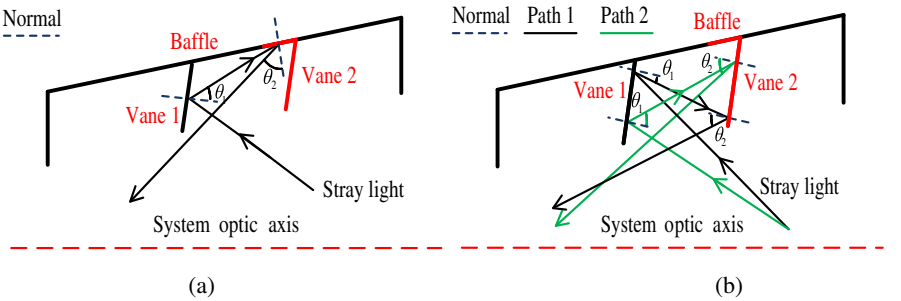

Fig. 5 Stray light propagation path: (a) vane–baffle propagation path and (b) vane–vane propagation path.

of the opposite vane is back-scatter (the scattering light and incident light are on the same side of the normal) light. As shown in Fig. 5, θ_1 represents the angle between the first-level scatter light and the normal and θ_2 represents the angle between the second-level scatter light and the normal.

Therefore, regardless of the propagation path, the second-level scatter light incident on the detector comes from the visible areas that must contain forward-scatter light and back-scatter light ($\theta_1 < 0$, $\theta_2 > 0$ or $\theta_1 > 0$, $\theta_2 < 0$). At this time, when the incident angle and vanes angle are determined, the BSDF distribution of second-level scatter light, as shown in Fig. 6, shows that most of the second-level scatter BSDF values are concentrated in the first quadrant (the first-level scatter light of vane is forward-scatter light, and the second-level scatter light of baffle is also forward-scatter light, $\theta_1 > 0$, $\theta_2 > 0$), and its value changes quickly as the angle (θ_1, θ_2) changes. In contrast, for the second quadrant ($\theta_1 < 0, \theta_2 > 0$) and the fourth quadrant ($\theta_1 > 0, \theta_2 < 0$), the BSDF values vary little and slowly; specifically, as the angle (θ_1, θ_2) changes, the range of change with the angle (θ_1, θ_2) is about 1%.

Therefore, we consider that the BSDF model that can scatter to the detector (as shown in Fig. 5) does not change with scattering angles (θ_1, θ_2) and uses the mean (the second quadrant and the fourth quadrant) to replace the second-level scatter BSDF value for each point (stray light can scatter to the detector), and the second-level scatter BSDF model is expressed as follows:

$$F(\theta_I, \theta_V) = \frac{\sum_N \mathrm{BSDF1}_i \mathrm{BSDF2}_i}{N}, \tag{8}$$

where θ_I is the incident angle and θ_V is the angle of the vane and baffle, $\mathrm{BSDF1}_i$ is the BSDF value of vane 1 at the different incident angles of stray light, and $\mathrm{BSDF2}_i$ is the BSDF value of vane 2 (opposite vane) and the baffle from vane 1 at different first-level scatter angles.

3.2 *Second-Level Scatter Irradiance Propagation Model*

In this section, we establish the model of E_I in Eq. (6) combining with the above analysis and irradiance propagation equation.

The irradiance propagation model is shown in Fig. 7. In the plane, the irradiance of microfacet S_2 can be expressed as

$$E = \int_{\gamma_1}^{\gamma_2} L_s \cos\gamma \sin\gamma \mathrm{d}\gamma, \tag{9}$$

where n_1, n_2 are the normals of the surfaces S_1, S_2, respectively, γ_1, γ_2 are the angles between the normal of microfacet S_2 and the direction of light propagation, L_s is the radiance of the surface S_1 at different directions, and ε is the angle of incidence.

According to the definition of BSDF, Eq. (9) can be written as follows:

$$E = E_I \int_{\gamma_1}^{\gamma_2} \mathrm{BSDF}(\varepsilon, \gamma) \cos\gamma \sin\gamma \mathrm{d}\gamma, \tag{10}$$

where E_I is the irradiance incident on surface S_1.

Therefore, based on the second-level scatter irradiance propagation model, E_i can be expressed as Eq. (11), where θ_I is the incident angle of stray light, θ_V is the angle of vane, α is the angle between the first-level scatter light and normal, and β is the angle between the second-level scatter light and normal:

$$E_i = E_b \int_{\kappa_i}^{\kappa_{i+1}} \left[\int_{\alpha_{\min}}^{\alpha_{\max}} \mathrm{BSDF}_1(\theta_I, \alpha) \cos\alpha \sin\alpha \mathrm{d}\alpha \right] \times \mathrm{BSDF}_2(\alpha', \beta) \cos\beta \sin\beta \mathrm{d}\beta. \tag{11}$$

Based on Eq. (11) and two kinds of propagation paths of the second-level scatter light incident on the detector, Eq. (11) can be written as follows:

$$\begin{aligned} E_i(\theta_I, \theta_V) &= E_b \int_{\kappa_i}^{\kappa_{i+1}} \int_{\alpha_{\min}}^{\alpha_{\max}} \mathrm{BSDF}_1(\theta_I, \alpha) \mathrm{BSDF}_2(\alpha', \beta) \\ &\quad \times \cos\alpha \sin\alpha \mathrm{d}\alpha \cos\beta \sin\beta \mathrm{d}\beta \\ E_i(\theta_I, \theta_V) &= E_b F(\theta_I, \theta_V) \int_{\kappa_i}^{\kappa_{i+1}} \left(\int_{\alpha_{\min}}^{\alpha_{\max}} \cos\alpha \sin\alpha \mathrm{d}\alpha \right) \\ &\quad \times \cos\beta \sin\beta \mathrm{d}\beta, \end{aligned} \tag{12}$$

where E_b denotes the irradiance of entering the baffle at stray light exclusive angle, $\mathrm{BSDF}_1(\theta_1, \alpha)$ is the BSDF that is incident on the visible region (the red part of Fig. 1) after stray light is scattered once, $\mathrm{BSDF}_2(\alpha', \beta)$ is the BSDF that is incident on the lens from the visible region (the red part of Fig. 1) after the stray light is scattered twice, α is the scattering angle of the first-level scatter light scattered into the visible region, and β is the scattering angle of the second-level scatter light scattered from the visible region to the lens.

According to the baffle structure, as shown in Fig. 1 and the light propagation path, as shown in Fig. 5, the first-level

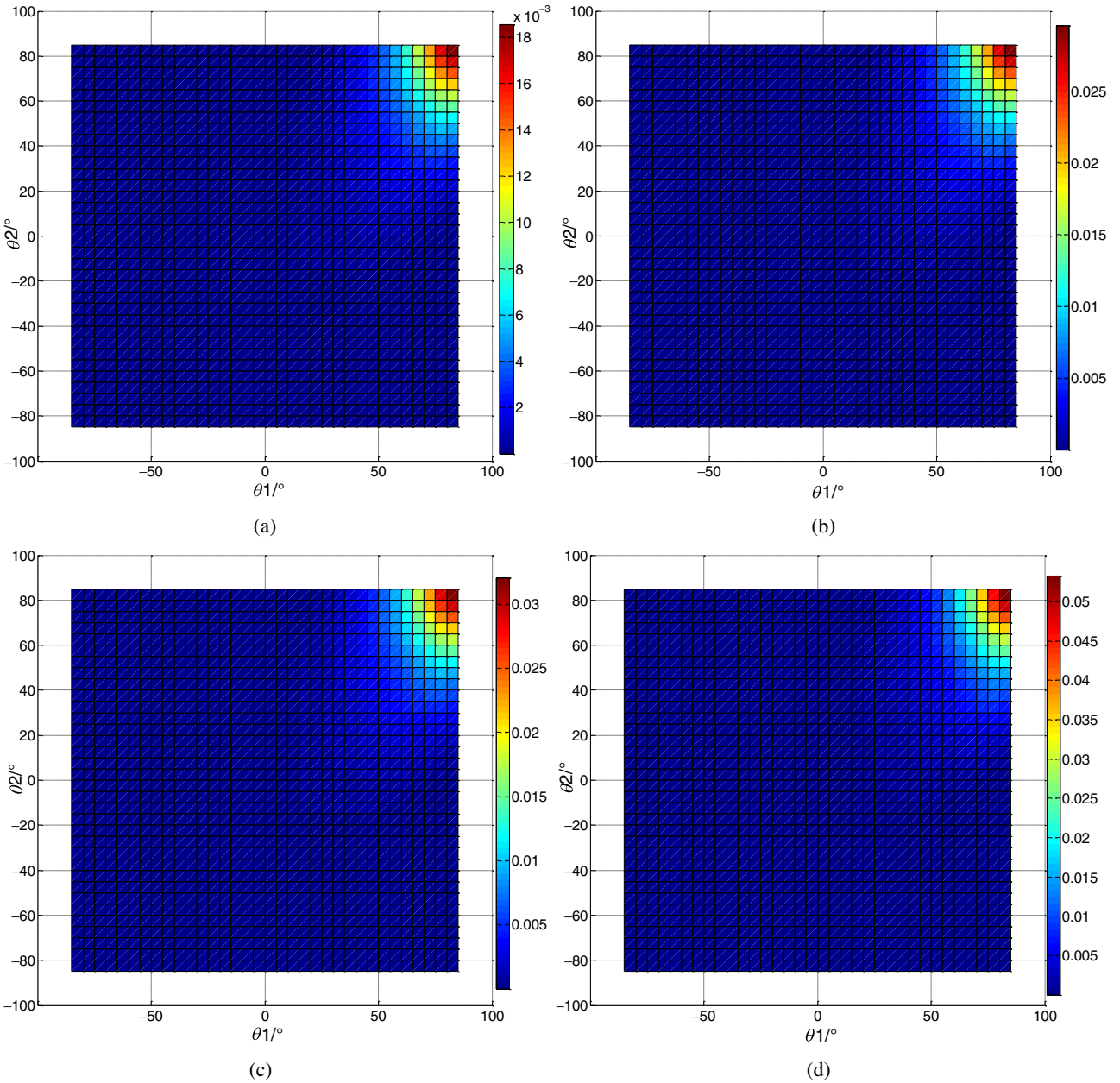

Fig. 6 The BSDF distribution of second-level scatter light is at different incidence angles: (a) the angle of incidence is 50 deg and (b) the angle of incidence is 60 deg. The BSDF distribution of second-level scatter light is at different vane angles: (c) the angle of vane is 55 deg and (d) the angle of vane is 57 deg.

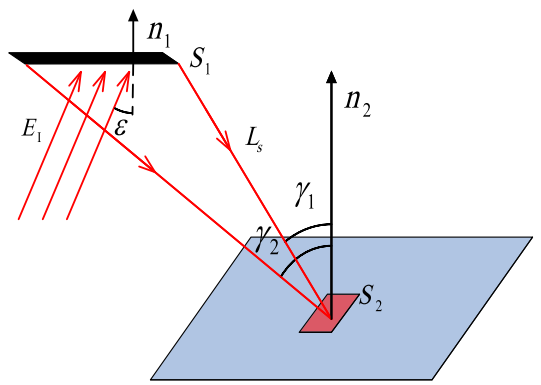

Fig. 7 Irradiance propagation model.

scatter light propagation model is from the vane to the opposite vane, as shown in Fig. 8.

In the case shown in Fig. 8(a), the expression of $f_1(\alpha) = \int_{\alpha_{\min}}^{\alpha_{\max}} \cos\alpha \sin\alpha \, d\alpha$ is as follows:

$$\begin{cases} f_1(\alpha) = \int_{\alpha_1}^{\alpha_2} \cos\alpha \sin\alpha \, d\alpha \\ f_1(\alpha) = \frac{1}{2}(\sin^2\alpha_2 - \sin^2\alpha_1) \end{cases}$$
$$\begin{cases} \sin^2\alpha_1 = \frac{(D\cot\theta_V + x - S)^2}{(D\cot\theta_V + x - S)^2 + D^2} \\ \sin^2\alpha_2 = \frac{(D\cot\theta_V + x)^2}{(D\cot\theta_V + x)^2 + D^2}. \end{cases} \tag{13}$$

In the case shown in Fig. 8(b), the expression of $f_2(\alpha) = \int_{\alpha_{\min}}^{\alpha_{\max}} \cos\alpha \sin\alpha \, d\alpha$ is as follows:

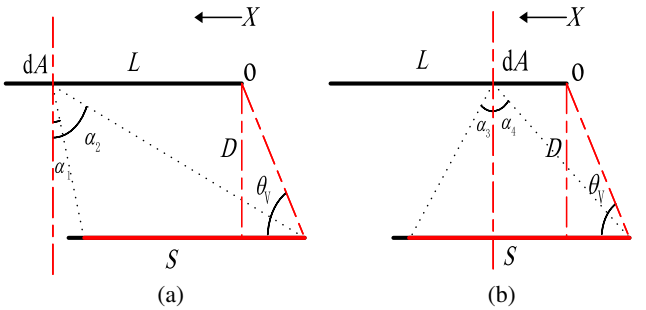

Fig. 8 (a) The area (S) of vane illuminated by the incident stray light is on the same side of opposite-vane microfacet normal and (b) the area (S) of vane illuminated by the incident stray light is on both sides of opposite-vane microfacet normal. Surface scattering without vanes.

$$\begin{cases} f_2(\alpha) = \int_0^{\alpha_3} \cos\alpha \sin\alpha \, \mathrm{d}\alpha + \int_0^{\alpha_4} \cos\alpha \sin\alpha \, \mathrm{d}\alpha \\ f_2(\alpha) = \frac{1}{2}(\sin^2\alpha_3 + \sin^2\alpha_4) \end{cases}$$
$$\begin{cases} \sin^2\alpha_3 = \frac{(S-x-D\cot\theta_V)^2}{(S-x-D\cot\theta_V)^2+D^2} \\ \sin^2\alpha_4 = \frac{(x+D\cot\theta_V)^2}{(x+D\cot\theta_V)^2+D^2}. \end{cases} \tag{14}$$

The first-level scatter light propagation model from the vane to the baffle visible area, as shown in Fig. 9.

In the case shown in Fig. 9, the expression of $f_3(\alpha) = \int_{\alpha_{\min}}^{\alpha_{\max}} \cos\alpha \sin\alpha \, \mathrm{d}\alpha$ is as follows:

$$\begin{cases} f_3(\alpha) = \int_{\alpha_5}^{\alpha_6} \cos\alpha \sin\alpha \, \mathrm{d}\alpha \\ f_3(\alpha) = \frac{1}{2}(\sin^2\alpha_6 - \sin^2\alpha_5) \end{cases}$$
$$\begin{cases} \sin^2\alpha_5 = \frac{[(L-S)\sin\theta_V]^2}{[(L-S)\sin\theta_V]^2+\{[x+(L-S)\cos\theta_V]\}^2} \\ \sin^2\alpha_6 = \frac{L^2\sin^2\theta_V}{L^2\sin^2\theta_V+(x+L\cos\theta_V)^2}, \end{cases} \tag{15}$$

where L is the length of the vane, D is the distance between the vanes, S is the length of the vane illuminated by the incident stray light, and O is the origin of the x axis. Similarly, the second-level scatter light incident on the detector from each visible area can also be obtained in the same way. Then we can calculate E_i from each cavity using the above method. Finally, the minimized PST can be calculated, and we can optimize the vane angle based on this result.

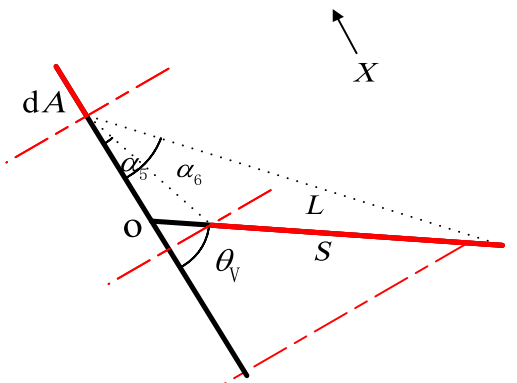

Fig. 9 The first-level scatter light propagation model from the vane to the baffle.

4 Results and Analysis

Using the model established in Sec. 3.2, we can calculate the PST of the x direction FOV and the y direction FOV separately, and we can calculate the PST of the system for the vane at different angles. The PST changes with the angle of the vane, as shown in Figs. 10(a) and 10(b).

To verify the correctness of the model method, the PST was simulated by the Monte Carlo ray-tracing method in LightTools, which is a ray-tracing software. The irradiance of entering the baffle is 1 W/mm^2, the absorptivity of the baffle and vane is 95%, and the scattering characteristics of baffle and vane comply with the BSDF model in Sec. 2.2. The simulation results of PST are shown in Figs. 11(a) and 11(b).

Comparing Fig. 10(a) with Fig. 11(a) and Fig. 10(b) with Fig. 11(b), respectively, shows that the model calculation result is of the same order of magnitude as the Monte Carlo ray-tracing simulation, and the trend of PST variation with the vane angle is the same in calculation and simulation. Given that dispersed light in stereoscopic space and the light scattered more than two times are not considered in this model method and the number of simulation rays also affects the simulation result, the results at the same point are slightly different for the two methods. However, it has no effect on the optimization of vane structure, and the error rapidly decreases with an increased FOV; the main reason for this effect is that as the incidence angle increases, more and more scattering light is concentrated in the incident plane, so the effect of dispersed light in stereoscopic space becomes smaller and smaller. As shown in Figs. 10 and 11, the error in the y direction FOV is much smaller than the error in the x direction FOV.

In addition, we need to design different mechanical structures and simulation environments for each vane structure to achieve the simulation result in the tradition ray-tracing method, and it is very time-consuming. However, the model calculation method can complete the optimization of the vane structure in a few minutes.

The traditional vane structure is a vertical structure; that is, the vane and optical axis are vertical, and in the x direction and y direction the angle with the baffle is 75 deg and 55 deg, respectively. However, using the optimization method proposed in this paper, when the angles are 83 deg and 62 deg, respectively, the PST can be reduced by two times and nearly five times at stray light exclusive angles, respectively. When the incident irradiance is 1 W/mm^2, the simulation results of irradiance distribution on the detector before and after optimization in LightTools are shown in Figs. 12(a)–12(d).

5 Conclusions

In this paper, we designed an angled and parallel vane structure under the limitation of a miniaturized baffle, and a rapid optimization model of vane structure was proposed based on the radiation transfer equation and the scattering characteristics of the material surface to improve the performance of stray light suppression in the space-based system. In addition, we verified the correctness of the optimization model by the Monte Carlo ray-tracing method in LightTools. Moreover, the vane structure was designed by applying this optimization model, and the PST was improved by two times in the x direction FOV and nearly five times in the y direction FOV when the angle of incidence was at the stray light exclusive angle

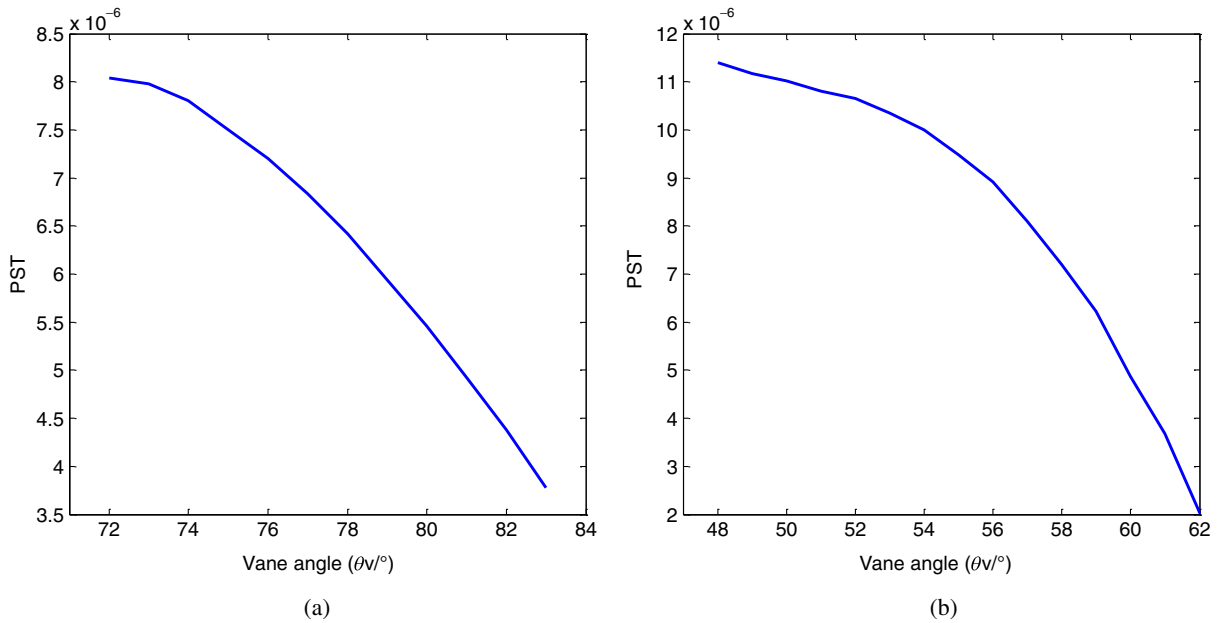

Fig. 10 (a) The model calculation results of the PST curve in the *x* direction FOV with an incident angle of 50 deg and (b) the model calculation results of the PST curve in the *y* direction FOV with an incident angle of 70 deg.

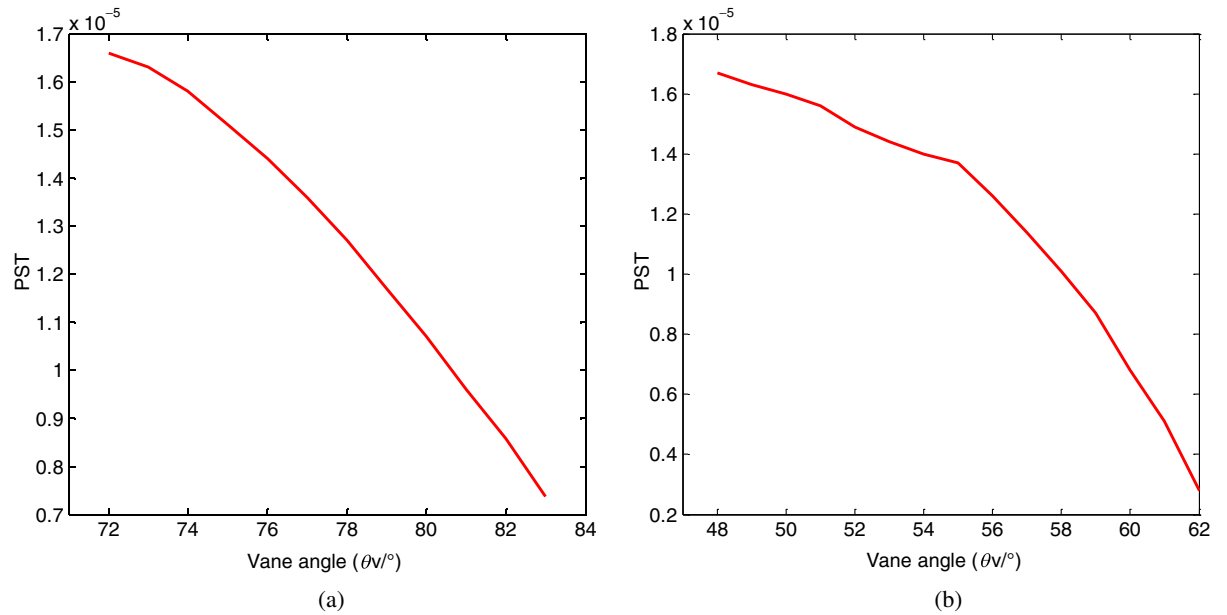

Fig. 11 (a) The simulation results of the PST curve in the *x* direction FOV with an incident angle of 50 deg and (b) the simulation results of the PST curve in the *y* direction FOV with an incident angle of 70 deg.

compared with the traditional method. In addition, the optimized baffle has a small length of 80 mm instead of 98 mm without decreasing light-shielding performance. Although there is a certain error in this optimization method, it does not affect the optimal design of the vane structure, and the errors gradually decrease with the increased FOV. Because the surface scattering model is established instead of the Lambert scattering, it can make the calculation and simulation results closer to the actual situation, especially in the wide FOV. In addition, because the optimized vane structure is still parallel, it does not cause difficulties in processing. Compared with the traditional method, this method establishes an analytical expression; therefore, the result is accurate and the time required for simulation can significantly be reduced. In a word, shrinking the volume of the baffle without decreasing stray light suppression performance is a common problem because the light-shielding baffle occupies a large volume in the space-based system with a wide FOV. This method provides an effective and rapid quantitative design method for solving this problem.

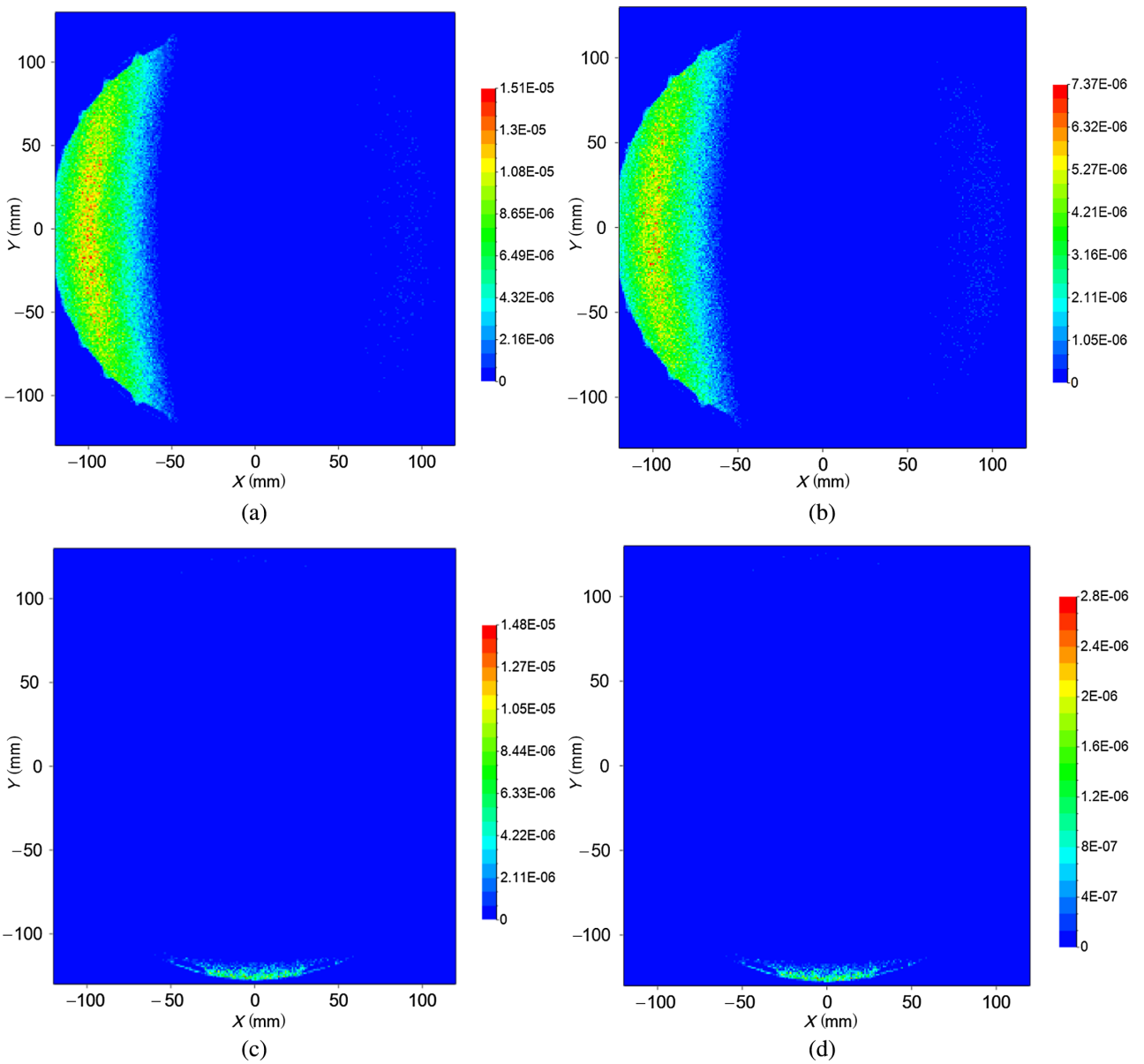

Fig. 12 (a) Irradiance distribution with a 75-deg vane angle at a 50-deg FOV, (b) irradiance distribution with an 83-deg vane angle at a 50-deg FOV, (c) irradiance distribution with a 55-deg vane angle at a 70-deg FOV, and (d) irradiance distribution with a 62-deg vane angle at a 70-deg FOV.

Acknowledgments

This work was supported in part by the National Key Research and Development Program of China under Grant No. 2016YFF0103603; the Technology Development Program of Jilin Province, China, under Grant No. 20180201012GX; and the National Natural Science Foundation of China under Grant Nos. 61627819, 61727818, and 6187030909.

References

1. X.-X. Zhang et al., "Wide-field auroral imager onboard the Fengyun satellite," *Light Sci. Appl.* **8**(47), 1–12 (2019).
2. R. K. Huebschman, "The MSX spacecraft system design," *John Hopkins APL Tech. Digest* **17**(1), 41–48 (1996).
3. A. T. Stair, Jr and J. D. Mill, "The MSX spacecraft system design," in *IEEE Int. Conf. Aerosp.*, pp. 233–245 (1997).
4. J. Sharma et al., "Toward operational space-based space surveillance," *Lincoln Lab. J.* **13**(2), 309–334 (2002).
5. E. M. Gaposchkin, C. von Braun, and J. Sharma, "Space-based space surveillance with the spaced-based visible," *J. Guidance Control Dyn.* **23**(1), 148–152 (2000).
6. G. P. Ellrod and R. V. Achutuni, "An assessment of GOES-8 imager data quality," *Bull. Am. Meteorol. Soc.* **79**(11), 2509–2526 (1998).
7. G. Wang et al., "Optimization method of star tracker orientation for sunsynchronous orbit based on space light distribution," *Appl. Opt.* **56**, 4480–4490 (2017).
8. G. Wang et al., "Optimization method for star tracker orientation in the sun-pointing mode," *Chin. Opt. Lett.* **15**, 081201 (2017).
9. A. Buffington, B. V. Jackson, and P. P. Hick, "Space performance of the multistage labyrinthine SMEI baffle," *Proc. SPIE* **5901**, 590118 (2005).
10. R. P. Breault, "Problems and techniques in stray radiation suppression," *Proc. SPIE* **0107**, 2–23 (1977).
11. R. P. Breault, "Vane structure design trade-off and performance analysis," *Proc. SPIE* **0967**, 90–117 (1989).
12. W. I. Linlor, "Optical system with reflective baffles," U.S. Patent No. 4,542,963 A (1984).
13. S. Kendrick, R. Kovacs, and A. L. Vaglia, "Solar simulation for testing off-axis light attenuation of a star sensor assembly," *Proc. SPIE* **0107**, 150–157 (1977).

14. V. Isbrucker et al., "Stray light control for asteroid detection at low solar elongation for the NEOSS at micro-satellite telescope," *Proc. SPIE* **8442**, 84424J (2012).
15. J. Haghshenas, "A theoretical method for vanes profile design in star sensor baffle," *Proc. SPIE* **9264**, 92641R (2014).
16. R. Saleem and S. Lee, "Reflective curved baffle for micro star trackers," in *Proc. IEEE Int. Symp. Robot. Intell. Sens.*, Ottawa, Ontario, pp. 5–7 (2017).
17. S. M. Pompea, "Star sensor baffle optimization: some helpful practical design rules," *Proc. SPIE* **2684**, 333–338 (1996).
18. G. Wang et al., "Rapid optimization method of the strong stray light elimination for extremely weak light signal detection," *Opt. Express* **25**(21), 26175–26185 (2017).
19. R. D. Seals and M. B. Mcintosh, "Advanced baffles: knife-edged diffuse-absorptive and dual reflective baffles," *Proc. SPIE* **1753**, 196–209 (1993).
20. S. R. Meier, "Methods to suppress stray light in black materials," *Proc. SPIE* **5526**, 195–207 (2004).
21. Y. Sun, "Statistical ray method for deriving reflection models of rough surfaces," *J. Opt. Soc. Am. A* **24**(3), 724–744 (2007).
22. J. C. Stover and J. E. Harvey, "Unified scatter model for rough surfaces at large incident and scatter angles," *Proc. SPIE* **6672**, 66720B (2007).
23. J. E. Harvey, A. Krywonos, and C. L. Vernold, "Modified Beckmann-Kirchhoff scattering model for rough surfaces with large incident and scattering angles," *Opt. Eng.* **46**(7), 078002 (2007).
24. I. G. E. Renhorn and G. D. Boreman, "Analytical fitting model for rough-surface BRDF," *Opt. Express* **16**(17), 12892–12898 (2008).
25. S. Schröder et al., "Modeling of light scattering in different regimes of surface roughness," *Opt. Express* **19**, 9820–9835 (2011).
26. I. Stamenov, I. P. Agurok, and J. E. Ford, "Optimization of two-glass monocentric lenses for compact panoramic imagers: general aberration analysis and specific designs," *Appl. Opt.* **51**(31), 7648–7661 (2012).
27. I. Stamenov et al., "Panoramic monocentric imaging using fiber-coupled focal planes," *Opt. Express* **22**(26), 31708–31721 (2014).
28. S. J. Olivas et al., "Image processing for cameras with fiber bundle image relay," *Appl. Opt.* **54**, 1124–1137 (2015).
29. H. Kawano et al., "Suppression of sun interference in the star sensor baffling stray light by total internal reflection," *Proc. SPIE* **5962**, 59621R (2005).

Zeming Xu received his BS degree in physics from Shandong University, Jinan, China, in 2016. He is currently pursuing his PhD at Changchun Institute of Optics, Fine Mechanics, and Physics, Chinese Academy of Sciences, Changchun, China. His research interests include stray light suppression, weak target detection, and image processing.

Chunhui Hu received his PhD in optical engineering from Changchun Institute of Optics, Fine Mechanics, and Physics, Chinese Academy of Sciences, Changchun, China, in 2013. He is the assistant researcher at Changchun Institute of Optics, Fine Mechanics, and Physics of the Chinese Academy of Sciences. His current research interests include installation and inspection of optical systems.

Changxiang Yan received his MS degree in engineering from Zhejiang University, Zhejiang, China, in 1998 and his PhD from Changchun Institute of Optics, Fine Mechanics, and Physics, Chinese Academy of Sciences, Changchun, China, in 2001. He is the director at the Space Optics Laboratory of Changchun Institute of Optics, Fine Mechanics, and Physics of the Chinese Academy of Sciences. His research interests include optomechatronics technology for space optical remote sensing instruments, multispectral and hyperspectral spatial remote sensing imaging, polarization detection, and space surveillance.

Cang Gu is the associate researcher at Changchun Institute of Optics, Fine Mechanics, and Physics of the Chinese Academy of Sciences. His current research interests include optical system processing and inspection.